doi:10.1016/j.jmb.2007.01.064 J. Mol. Biol. (2007) 368, 407–420

JMB

Available online at www.sciencedirect.com

ScienceDirect

ELSEVIER

The Structure of the KinA-Sda Complex Suggests an Allosteric Mechanism of Histidine Kinase Inhibition

Andrew E. Whitten[2]†, David A. Jacques[1]†, Boualem Hammouda[3] Tracey Hanley[2], Glenn F. King[4], J. Mitchell Guss[1], Jill Trewhella[1,5] and David B. Langley[1]*

[1]*School of Molecular and Microbial Biosciences University of Sydney Sydney 2006, Australia*

[2]*Bragg Institute, Australian Nuclear Science and Technology Organisation Lucas Heights 2234, Australia*

[3]*National Institutes of Standards and Technology MD 20899, USA*

[4]*Department of Molecular Microbial and Structural Biology, University of Connecticut Health Center Farmington, CT 06030, USA*

[5]*Department of Chemistry University of Utah, Salt Lake City, UT 84112, USA*

**Corresponding author*

The *Bacillus subtilis* histidine kinase KinA controls activation of the transcription factor governing sporulation, Spo0A. The decision to sporulate involves KinA phosphorylating itself on a conserved histidine residue, after which the phosphate moiety is relayed *via* two other proteins to Spo0A. The DNA-damage checkpoint inhibitor Sda halts this pathway by binding KinA and blocking the autokinase reaction. We have performed small-angle X-ray scattering and neutron contrast variation studies on the complex formed by KinA and Sda. The data show that two Sda molecules bind to the base of the DHp dimerization domain of the KinA dimer. In this position Sda does not appear to be able to sterically block the catalytic domain from accessing its target histidine, as previously proposed, but rather may effect an allosteric mode of inhibition involving transmission of the inhibitory signal *via* the four-helix bundle that forms the DHp domain.

Keywords: histidine kinase; KinA; Sda; small-angle scattering; neutron contrast variation

Introduction

Histidine kinases are enzymes predominantly employed by bacteria as components of signal transduction pathways that orchestrate cellular responses to environmental stimuli. Typically, each histidine kinase functions in concert with a transcription factor, termed the response regulator.[1] When a histidine kinase recognizes its cognate signal, usually a small effector molecule, it autophosphorylates by transferring the terminal phosphate of ATP to a conserved histidine residue to form a phosphoimidazole adduct. This phosphate moiety is subsequently transferred to a conserved aspartate residue on the response regulator, inducing a conformational change that leads to the up or down-regulation of an ensemble of target genes. Responses governed by such pathways are as disparate as chemotaxis, nutrient utilization, and the specialized cell division process known as sporulation that is undertaken by certain species of bacteria. Sporulation occurs specifically in response to starvation and involves an asymmetric cell division in which one daughter chromosome is pack-

† A.E.W. and D.A.J. contributed equally to this work.

Present address: G. F. King, Division of Chemical and Structural Biology, Institute for Molecular Bioscience, The University of Queensland, St. Lucia, QLD 4072, Australia.

Abbreviations used: CA, catalytic and ATP-binding domain of KinA; DHp, dimerization and histidine phosphotransfer domain of KinA; D_{max}, maximum linear dimension; $KinA_2$, KinA dimer; Sda_2, Sda dimer; ^{D}Sda, deuterated Sda; $KinA_2$-2Sda, KinA dimer with two bound Sda molecules; $KinA_2$-2^{D}Sda, KinA dimer with two bound deuterated Sda molecules; PDB, Protein Data Bank; R_g, radius of gyration; GST, glutathione-*S*-transferase.

E-mail address of the corresponding author: d.langley@mmb.usyd.edu.au

aged into a resilient spore that can survive until conditions are favorable for germination.

The primary histidine kinase responsible for activating the sporulation pathway in *Bacillus subtilis* is KinA. Once activated, KinA indirectly phosphorylates its cognate response regulator, the transcription factor Spo0A, *via* a phosphorelay involving two additional proteins, Spo0F and Spo0B.[2] The phosphate moiety on KinA is transferred to an aspartate residue on Spo0F, from the Spo0F aspartate to a histidine on Spo0B, then from the Spo0B histidine to an aspartate on Spo0A, thereby activating it. Hence, the γ-phosphate of ATP is passed from: ATP→His→Asp→His→Asp. The increased complexity of this phosphorelay, compared to the more typical two-component pathway employed by most histidine kinases, provides more points at which a decision as important as sporulation can be regulated. As packaging damaged genetic material might compromise the production of viable spores, a mechanism exists to halt the onset of sporulation when DNA-damage is detected. In response to DNA damage a small 46 residue protein known as Sda,[3] whose structure has been solved using NMR,[4] is up-regulated along with the many proteins involved in DNA repair and recombination. Sda binds KinA and prevents its autokinase activity, thus silencing the sporulation directive at the first step of the KinA-Spo0A phosphorelay.[4] Interestingly, while Sda inhibits the KinA autophosphorylation reaction, it does not abrogate the ability of already phosphorylated KinA to donate phosphate to Spo0F.

Histidine kinases generally have two domains: an N-terminal "sensor" domain, often membrane-bound, which recognizes one or more signal molecules, and a C-terminal "autokinase" domain. The autokinase domain is further divided into a C-terminal catalytic and ATP-binding (CA) domain and an N-terminal dimerization and histidine phosphotransfer (DHp) domain (Figure 1(a)). KinA is comprised of 606 amino acid residues, the first 383 of which constitute the sensor region which contains three Per-Arnt-Sim (PAS) domains[5] to which as-yet-unknown effector molecules presumably bind. Residues 383–606 constitute the autokinase half of the protein, with residues 383–465 and 456–606 forming the DHp and CA domains, respectively. Although the structure of the autokinase domain of KinA has not been solved, it can be modeled using the structures of homologues. The structures of isolated CA domains are known from the histidine kinases EnvZ,[6] NtrB,[7] and PhoQ[8] from *Escherichia coli*, CheA from *Thermotoga maritima*,[9] and PrrB from *Mycobacterium tuberculosis*.[10] All display the same α/β sandwich fold. The structure of the isolated DHp domain from EnvZ[11] reveals a helix-turn-helix fold (involving helices α1 and α2), which in the context of its dimer partner (helices α1′ and α2′) forms a four helix bundle or "stalk"(Figure 1(b)). Approximately halfway along the stalk on the α1 and α1′ helices lie the solvent-orientated target histidine residues. When the sensor domain is appropriately stimulated, the CA domains catalyze a *trans*-autophosphorylation reaction in which each CA domain phosphorylates the target histidine on the opposite protomer. Disulfide cross-linking studies of the EnvZ autokinase domain have led to a model predicting the positions of the DHp and CA domains during the autophosphotransfer event.[12] Recently, the first crystal structure of an entire histidine kinase autokinase domain, designated HK853, from *T. maritima* was solved.[13] The HK853 structure has its canonical CA domains and DHp stalk positioned in an "extended" conformation such that considerable movement of the CA domains would be required to facilitate autokinase activity (Figure 1(b)).[13] This arrangement is one that allows for the interaction of the histidine kinase with the response regulator, which must access the same target histidine. A similar extended arrangement of CA and DHp domains is noted in a model derived from low resolution X-ray diffraction and small-angle X-ray scattering of the ThkA-TrrA HK-RR complex from *T. maritima*.[14]

Two molecules of Sda bind to a dimer of KinA ($KinA_2$), to form a $KinA_2$-2Sda heterotetramer, and in doing so increase the stability of the $KinA_2$.[4] Whilst a combination of site-directed mutagenesis, pull-down and kinase assays identified the surface of Sda involved with binding KinA, little is known of the molecular surface of KinA to which Sda binds.[4] It has been proposed that Sda binds KinA at or near the "hinge" region linking the CA and DHp domains[4,15] (Figure 1(b)), and that anti-autokinase activity might be achieved by Sda acting as a "molecular barricade", sterically preventing the CA domain from accessing the target histidine.

We present here the results of small-angle solution scattering and neutron contrast variation experiments on the dimeric KinA autokinase domain, Sda and the complex they form. The data provide information on the shapes of the structures of the individual protein components alone in solution, as well as their shapes and dispositions within the $KinA_2$-2Sda complex. The Sda binding region identified on $KinA_2$ is toward the lower part of the stalk region with no direct interaction with the CA domains or the linker connecting the DHp and CA domain. These results suggest that the inhibitory signal involves a conformational change within the stalk region that affects the hinge region allosterically rather than being a simple molecular barricade.

Results and Discussion

Quality of protein samples and scattering data

Interpretation of small-angle scattering data in terms of structure requires samples that are rigorously monodisperse and approximate the conditions of dilute solution, i.e. there are no distance correlations among the scattering particles that can bias the structural parameters. Size-exclusion chromatography of KinA samples used for scattering experiments yielded a single peak, which dynamic light scattering

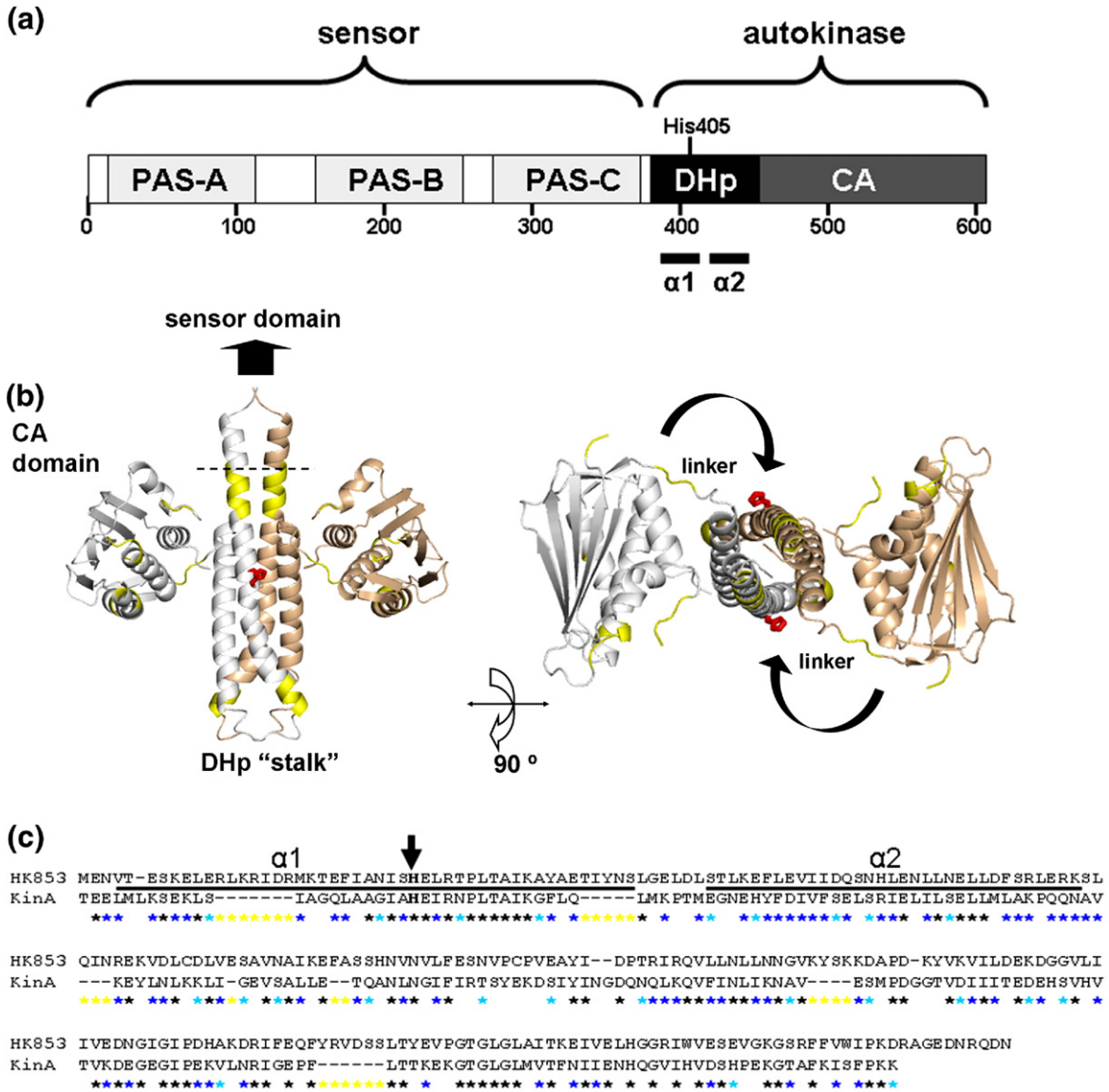

Figure 1. Histidine kinase domain architecture. (a) KinA is comprised of an N-terminal sensor region and a C-terminal autokinase region. The autokinase region is further subdivided into dimerization and phosphotransfer (DHp) and catalytic (CA) sub-domains. The histidine that becomes phosphorylated (His405) is located in the one of two helices within the DHp domain (indicated by bars). (b) HK853 structure comprising DHp stalk and CA domains. The movement that CA domains must undertake to phosphorylate target histidine residues (red sticks), is indicated by curved arrows (right panel). The dotted line (left panel) approximates the point at which HK853 was truncated to better model KinA. Segments colored yellow are missing from the KinA primary structure. (c) Alignment of amino acid sequences of HK853 (residues 232–489) and KinA (residues 383–606). Identical, conserved, weakly conserved and gap positions are indicated by black, blue, sky-blue and yellow markers, respectively. The arrow within helix α1 (bar) identifies the histidine targeted for phosphorylation.

confirmed to be consistent with a dimeric KinA having a mass of ~54 kDa (data not shown). Mass spectrometry gave a mass of 27,101 Da, as expected for the 6His-tagged KinA monomer with the N-terminal methionine removed. The molecular mass of Sda estimated from dynamic light scattering was ~13 kDa, suggesting that it is a dimer in solution under the chosen experimental conditions. The mass estimated for Sda from mass spectrometry was 5584 Da, as expected for the Sda monomer cleaved from its glutathione-*S*-transferase (GST) fusion partner.

The $KinA_2$-2Sda complex was prepared by combining $KinA_2$ with a stoichiometric excess of Sda and purifying it from excess Sda by size-exclusion chromatography. Mass spectrometry on resultant complex fractions repeatedly returned KinA-derived mass values of 25,350 Da, consistent with removal of the N-terminal 6His-tag from the KinA species. The expression constructs for both 6His-KinA and GST-Sda have a thrombin cleavage site to facilitate tag removal. Considerable amounts of thrombin were required to cleave GST from Sda. In contrast, as 6His-KinA was both hypersensitive to

thrombin activity and susceptible to undesired proteolysis, the 6His-tag was left uncleaved in the KinA preparations. Hence, the unexpected mass spectrometry data for the complex suggest that trace amounts of thrombin contaminating the gel filtration-purified Sda may have trimmed the 6His-tag from the KinA during complex formation and purification.

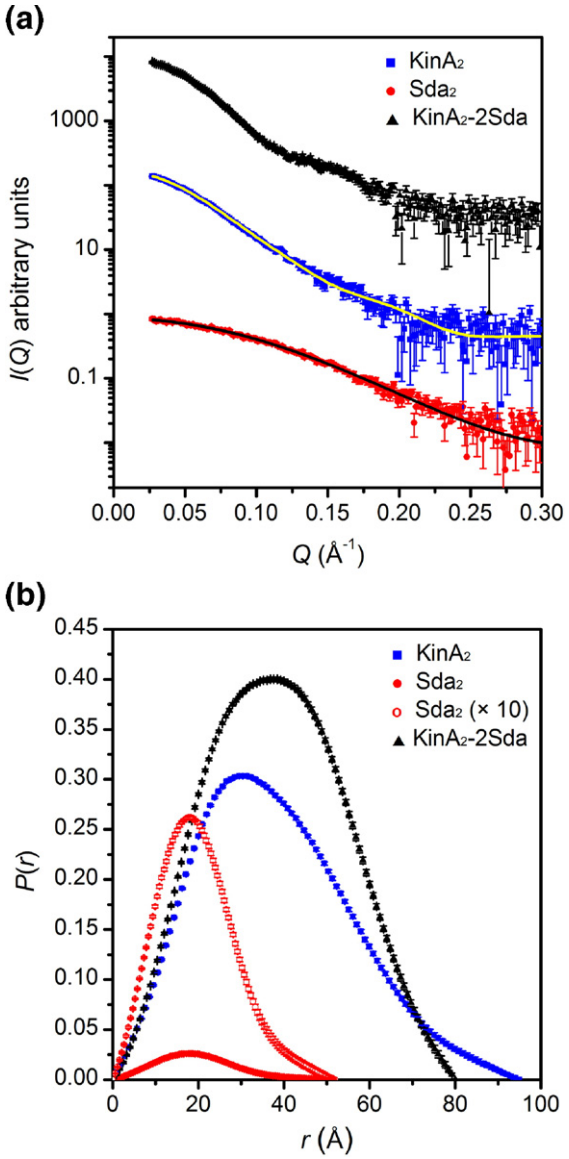

Figure 2. X-ray scattering profiles of $KinA_2$, Sda_2 and $KinA_2$-2Sda. (a) Background-subtracted scattering profiles for $KinA_2$ (blue), Sda_2 (red) and $KinA_2$-2Sda (black), where the plots have been shifted relative to each other for clarity. The fits obtained from rigid-body modeling based on the HK853 dimer structure and two molecules of Sda based on the NMR structure of the monomer are superimposed over the $KinA_2$ and Sda_2 scattering profiles. (b) $P(r)$ transformations of the scattering data for $KinA_2$, Sda_2 and $KinA_2$-2Sda (colored as in (a)). The $P(r)$ curves are scaled to reflect the number of vector lengths within the protein. The Sda trace has also been multiplied by a factor of 10 so that features of the curve can be seen.

The small-angle X-ray scattering profiles ($I(Q)$ *versus* Q, where $Q=4\pi(\sin\theta)/\lambda$) for KinA, Sda, and the complex they form are shown in Figure 2(a). Figure 2(b) shows the corresponding distance distribution functions, $P(r)$, calculated as the inverse Fourier transform of $I(Q)$ using the program GNOM.[16] The $P(r)$ function is the probable distribution of distances between scattering centers within the scattering particle and therefore goes to zero at its maximum dimension, D_{max}. The area under the $P(r)$ profile gives the zero angle or forward scattering, $I(0)$. The radius of gyration, R_g, can also be calculated from $P(r)$ (mathematically, it is the second moment of $P(r)$). Alternatively, R_g can be calculated using the lowest-Q data and the Guinier approximation.[17] The R_g is a summary measure of the distribution of distances of atoms from the center of the molecule. The agreement between the Guinier and $P(r)$-derived R_g values (Table 1) and the $I(0)$ analysis (discussed below) are excellent evidence that the samples were well-behaved, monodisperse particles in solution. In addition, the fit of the experimental data to the $P(r)$ model, determined using the regularisation technique employed in GNOM, gave goodness-of-fit values greater than 0.9 in all cases, indicating excellent agreement.

X-ray scattering data indicate that both Sda and KinA are dimers in solution

For a solution of monodisperse particles, $I(0)$ normalized for concentration (in mg/ml) and molecular weight is a constant. The values reported in Table 1 show that this requirement is met assuming that both KinA and Sda are homodimers in solution and that the complex they form has a 2:2 stoichiometry (Table 1). This $I(0)$ analysis is consistent with the R_g and D_{max} values derived from the $P(r)$ analysis. The experimental values determined for KinA agree well with those calculated for the homologous HK853 dimer (see discussion below, $R_g=28.9$ Å, $D_{max}=89$ Å, calculated using the program CRYSOL[18] and Protein Data Bank (PDB) coordinate file 2C2A). However, those measured for Sda are too large for a single Sda molecule ($R_g=11.5$ Å, $D_{max}=34$ Å calculated using CRYSOL and PDB coordinate file 1PV0). The program SASREF6[19] was used to perform rigid-body refinement of an Sda dimer, in which the position and orientation of two Sda monomers relative to each other were optimized, yielding a dimer model with an excellent fit to the X-ray data ($\chi^2=1.08$, Figure 2(a), black line on red data). Additionally, X-ray data acquired for Sda at concentrations as low as 1 mg/ml ($\cong 0.1$ mM) did not reveal evidence of dimer dissociation.

The shape of KinA is similar to HK853 and is compacted upon binding Sda

Among the available structures of histidine kinases, that from *T. maritima* (HK853 residues 232–489, PDB code 2C2A)[13] has the highest sequence

Table 1. Structural parameters derived from X-ray scattering data using Guinier and *P(r)* analyses

Protein	Concentration (mg/ml)	Guinier	*P*(*r*)		
		R_g (Å)	R_g (Å)	D_{max} (Å)	$I(0)/(c \times MW)$[a]
$KinA_2$	3.7	29.3±0.4	29.6±0.1	95	8.6±0.9
Sda_2	5.2	15.3±0.3	15.4±0.1	52	7.4±0.7
$KinA_2$-2Sda	4.4	29.2±0.3	29.10±0.06	80	7.4±0.7
$KinA_2$-2^{D}Sda	3.7	29.4±0.5	29.1±0.1	80	n.a.

[a] Assumes that KinA and Sda are dimers, and that the stoichiometry of the complex is 2:2.

homology with KinA (residues 383–606). The 258 residues of HK853 and 224 residues of KinA spanning these regions share 29% amino acid identity, 49% similarity, and contain only 10% of "gap" sequence (Figure 1(c)). Beyond the simple calculation of R_g and D_{max} values given above, theoretical scattering curves were derived from HK853-based models and compared with X-ray scattering data measured for $KinA_2$. Each HK853 monomer was first N-terminally truncated by seven residues to account for the large N-terminal homology gap noted in the DHp domain (Figure 1(b), dotted line and yellow helical segment immediately below this line). Rigid body modeling of this structure using SASREF6, in which the relative positions of the DHp and CA domains were optimized, provided an excellent fit to the $KinA_2$ X-ray scattering profile for this model (χ^2 of 1.04) (Figure 2(a), black line over blue data) with the extremities of the CA domains ~5 Å further apart than in the HK853 structure.

The X-ray scattering data also show that the binding of two Sda molecules to $KinA_2$, which constitutes an 11% increase in mass, results in a significantly smaller D_{max} value for the complex (reduced from 95 to 80 Å), while there is no change in the R_g value (Table 1). These results indicate that an overall compaction of $KinA_2$ must occur upon Sda binding, consistent with information from the neutron scattering experiments described below.

Neutron contrast variation data provide information on the shapes and dispositions of components within the $KinA_2$-2Sda complex

Neutron contrast variation experiments were performed with deuterated Sda (^{D}Sda) complexed with non-deuterated KinA in order to extract structural information on the individual components within the complex. The intensity of the small-angle scattering signal from proteins in solution depends upon their contrast, which is simply the difference in scattering density (ρ) between the protein and the solvent (i.e. contrast, $\Delta\rho = \rho_{protein} - \rho_{solvent}$). X-rays are scattered by electrons and X-ray scattering power therefore increases monotonically with atomic number. As most proteins have very similar elemental composition, they have similar electron densities and it is not generally possible to separate the contributions to a scattering profile from two proteins within a complex. Neutrons are scattered by atomic nuclei, and scattering power varies randomly with atomic number and isotopes of the same element can show large differences. One of the largest isotope differences is between the stable isotopes of hydrogen ($^1H \equiv H$ and $^2H \equiv D$, referred to as hydrogen and deuterium, respectively). This difference, combined with the facts that hydrogen is abundant in biomolecules and deuterium substitution in proteins and in their solvents can be relatively easy and benign, provides the opportunity for contrast variation experiments. By forming a protein complex in which one protein component is deuterated and measuring the neutron scattering profiles for the complex in solvents with different H:D ratios, the contrast of the individual protein components is systematically varied. From such a "contrast series," structural information on the individual components and their relative dispositions can be obtained.

The Sda was selected for deuteration due to its superior stability in solution compared with KinA. Deuterating Sda had the additional advantage of compensating for the relatively small size of the Sda, and hence its small scattering signal, by giving it a large contrast in solutions with high H content for which incoherent background scattering is also high. The ^{D}Sda was prepared by bacterial expression using deuterated media. Mass spectrometry indicated that the resultant ^{D}Sda had ~86% of non-exchangeable hydrogen positions deuterated.

Two neutron contrast series were measured for $KinA_2$-2^{D}Sda at different protein concentrations and with different salt concentrations: 3.7 mg/ml protein in 50 mM NaCl (contrast variation series not shown) and 11.9 mg/ml in 200 mM NaCl (Figure 3). The latter contrast series also included a measurement of the complex at 26.6 mg/ml in 40% D_2O at which value the neutron scattering density of KinA is approximately matched to that of the solvent and hence only the Sda molecules contribute to the scattering signal; i.e. the KinA has zero contrast and thus is "solvent matched." The values for R_g and D_{max} for both series are given in Table 2. The R_g data from the two independent contrast series with a ~threefold difference in protein concentration are in excellent agreement, indicating the absence of significant inter-particle interference. The increased salt concentration in the second contrast series measurement was explicitly done to minimize this potential effect that arises when there are inter-particle distance correlations in the solutions, often due to electrostatic repulsive forces, that give rise to a structure factor term. This term can suppress the lowest-angle data and bias

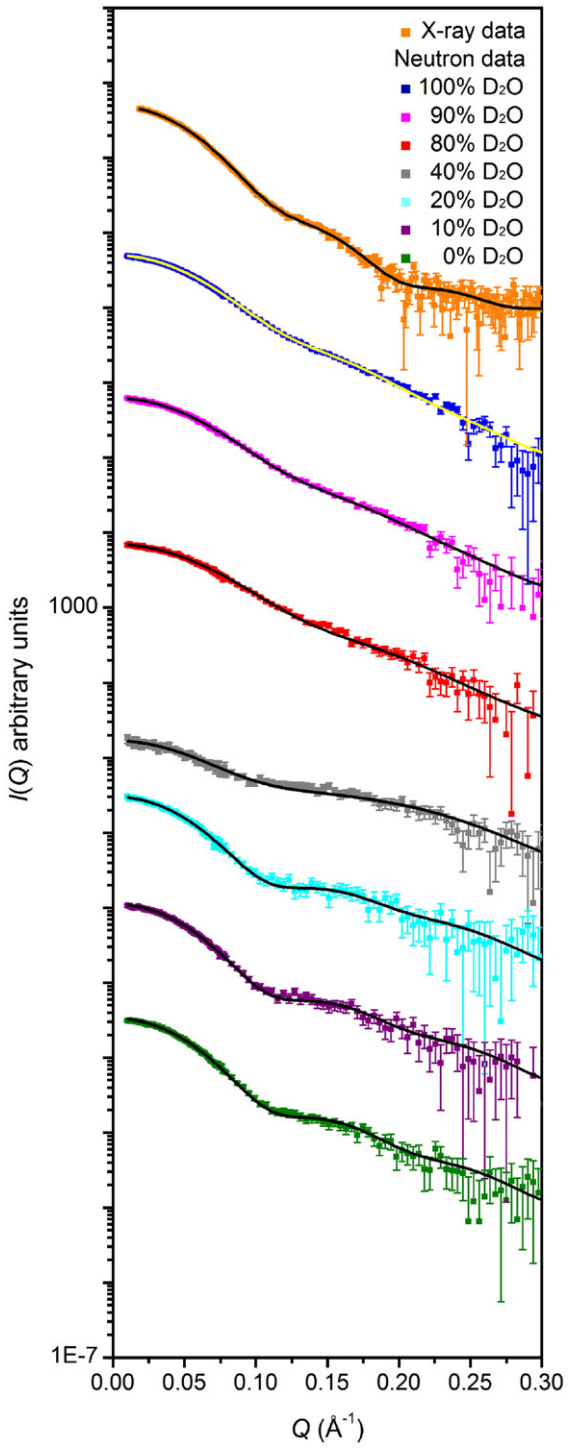

Figure 3. X-ray and neutron scattering profiles for the $KinA_2$-2^{D}Sda complex; the plots have been shifted relative to each other for clarity. Superimposed on the scattering profiles are the fits to the scattering data for our best-fit model based on rigid-body modeling using the HK853 dimer and Sda structures.

the derived structural parameters, thus making macromolecules appear smaller than they are. As an additional check, an X-ray scattering concentration series was measured on the samples used for the neutron studies. In these data a small concentration-dependent inter-particle interference effect in the 11.9 mg/ml samples was extracted and estimated to be 1.2% at $Q=0.02$ Å^{-1} and 0.003% at $Q=0.04$ Å^{-1}, well below the statistical quality of individual neutron scattering data sets.

Two different approaches were used to interpret the dependence of R_g on the mean contrast for the complex in terms of structural parameters for the components. The first is based on the work of Stuhrmann,[20] in which the R_g values for the complex are related to contrast by:

$$R_g^2 = R_m^2 + \frac{\alpha}{\Delta\bar{\rho}} - \frac{\beta}{\Delta\bar{\rho}^2}, \qquad (1)$$

where $\Delta\bar{\rho}$ is the mean contrast for the complex (equal to the volume fraction weighted sum of the contrast values for the KinA and ^{D}Sda components), R_m is the radius of gyration value of the complex at infinite contrast, and α and β are scattering density related coefficients. The sign of α relates to whether the center of mass of the component with the lowest or highest scattering density is closest to the center of mass of the entire complex, and β is proportional to the separation of the centers of mass of the two components. From these coefficients, R_g values for the $KinA_2$ and 2^{D}Sda components in the complex and the separation of their centers of scattering density can be calculated using the methods and equations that we have previously described in detail.[21] These parameters can also be determined from the parallel axis theorem.[21,22] A plot of the Stuhrmann relationship for the $KinA_2$-2^{D}Sda data (Figure 4) shows definite quadratic behavior that is extremely well represented by the fitted polynomial. The positive value observed for the coefficient α (corresponding to the position of the apex of the parabola being at positive values of $1/\Delta\bar{\rho}$) reveals that the higher contrast component (2^{D}Sda) lies towards the periphery of the complex. The structural parameters obtained from both analyses (Table 3) show that the distance between the centers of scattering density (which to a good approximation is the same as the centers of mass) is 27±1 Å, with R_g for the $KinA_2$ component equal to 25.5±0.2 Å and R_g for the 2^{D}Sda component equal to 25±1 Å.

Another method of analysing contrast variation data that uses all of the scattering data, as opposed to the summary R_g values, involves decomposition of the scattering profiles into contributions from the deuterated and non-deuterated components, and a "cross" term due to the proximity of these components in the complex.[21] Each scattering profile can be expressed in the form:

$$I^{exp}(Q,\Delta\rho_H,\Delta\rho_D) = \Delta\rho_H^2 I_H(Q) + \Delta\rho_D^2 I_D(Q) + \Delta\rho_H\Delta\rho_D I_{HD}(Q), \qquad (2)$$

where $\Delta\rho_H=\rho_H-\rho_{solvent}$, and is the contrast of the non-deuterated protein, and is the corresponding quantity for the deuterated protein at a given H:D ratio in the solvent. Contrast values are calculated from the amino acid sequence of the proteins, their

Table 2. Structural parameters derived from individual neutron scattering profiles using Guinier and *P(r)* analyses

Sample	Protein concentration (mg/ml)	% D_2O	Guinier R_g (Å)	*P(r)* R_g (Å)	*P(r)* D_{max} (Å)
$KinA_2$-$2^{D}Sda$	3.7	0	28.9±0.7	28.3±0.5	80
		10	28.3±1.1	28.5±0.9	80
		20	28.0±2.8	27.9±1.0	80
		70	15.4±1.7	15±8	80
		80	22.5±1.3	22.7±0.8	80
		90	27.1±0.7	24.4±0.3	80
		100	25.7±1.3	25.1±0.3	80
$KinA_2$-$2^{D}Sda$	11.9	0	28.3±0.2	28.9±0.1	80
		10	28.2±0.3	28.3±0.2	80
		20	29.1±0.5	28.2±0.3	80
		80	22.5±0.2	23.0±0.2	70
		90	24.3±0.1	24.2±0.1	75
		100	25.3±0.1	25.1±0.1	75
$KinA_2$-$2^{D}Sda$	26.6	40	21.6±0.6	23.4±0.7	70

estimated cumulative volumes,[23] and standard scattering lengths for the appropriate atoms contained within them. The scattering profiles I_H, I_D and I_{HD} are obtained by weighted least-squares fit to equation (2) at the different contrast values as described previously.[21] The scattering profiles obtained from this procedure and the corresponding *P*(*r*) profiles calculated using GNOM are displayed in Figure 5(a) and (b), respectively. The associated R_g values are seen to be in good agreement with those obtained independently from the Stuhrmann plot and the parallel axis theorem (Tables 2 and 3).

The *P*(*r*) profile obtained for the $2^{D}Sda$ component (Figure 5(b), filled and open red spheres) is characteristic of two separated globular molecules. Hence, although Sda molecules alone in solution exist as dimers, they bind to $KinA_2$ as monomers. The position of the second peak of the $2^{D}Sda$ profile also indicates that the centers of mass of the two Sda molecules are separated by approximately 45 Å. The extracted *P*(*r*) profile for the $KinA_2$ component (Figure 5(b), blue squares), and the associated R_g and D_{max} values (Table 3), as well as the X-ray scattering data (Table 1), all indicate that the $KinA_2$ in the complex is significantly more compact than free $KinA_2$ in solution (Figure 2(b)).

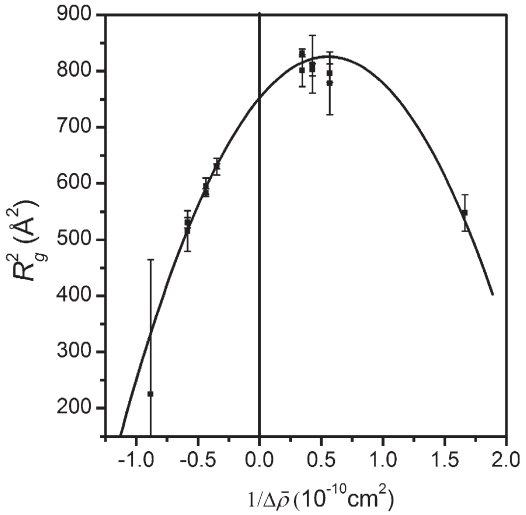

Figure 4. Stuhrmann plot for the $KinA_2$-$2^{D}Sda$ particle.

The neutron scattering data analysis presented thus far point towards a model for the $KinA_2$-$2^{D}Sda$ complex in which the ^{D}Sda components are positioned toward the periphery of the complex, the $KinA_2$ and $2^{D}Sda$ centers of mass are separated by ~27 Å, and the centers of the two ^{D}Sda molecules are 45 Å apart. These constraints place the individual ^{D}Sda molecules on opposite sides of the base of the DHp stalk of $KinA_2$. Two extreme orientations of the ^{D}Sda molecules with respect to the 2-fold axis down the DHp domain can be considered; one orientation has each ^{D}Sda molecule positioned directly under a CA domain, the other has them equidistant from the CA domains in a plane perpendicular to the first positions. Information regarding the correct orientation is encoded within the cross-term *P*(*r*) profile (Figure 5(b), green triangles). This plot represents the distribution of vector lengths between atoms in the non-deuterated $KinA_2$ and those in the two ^{D}Sda molecules. Theoretical profiles derived from the alternate arrangements are shown in Figure 6. The experimentally derived cross-term *P*(*r*) more closely resembles the theoretical profile derived from a model in which the ^{D}Sda molecules lie equidistant from the two CA domains, showing a single dominant peak at 40–45 Å. The shoulder evident at about 25 Å suggests that the ^{D}Sda molecules bind a little off center to the equidistant position.

Models for the $KinA_2$-$2^{D}Sda$ complex that satisfy all of the constraints derived from these basic analyses of the scattering data will have the ^{D}Sda molecules positioned on either side of the DHp domain of $KinA_2$ near the base and approximately equidistant from each of the catalytic domains.

Modeling the $KinA_2$-$2^{D}Sda$ complex against all the scattering data

A $KinA_2$-$2^{D}Sda$ model consisting of our truncated HK853 dimer (described above) and two

Table 3. Structural parameters for the components of the $KinA_2$-$2^{D}Sda$ complex from three different analyses of the neutron contrast series data

	$KinA_2$ in the complex		^{D}Sda in the complex		
	R_g (Å)		R_g (Å)		D^a (Å)
Stuhrmann analysis	25.43±0.08		25.31±0.67		27.0±1.0
Parallel axis theorem	25.51±0.08		25.59±0.65		26.6±1.0
	R_g (Å)	D_{max} (Å)	R_g (Å)	D_{max} (Å)	
Component scattering functions	25.2±0.1	75	25.1±0.5	75	

[a] D is the separation of the centres of scattering density (or mass) for the $KinA_2$ and $2^{D}Sda$ components.

monomeric Sda molecules (coordinates from the NMR structure, PDB 1PV0) was subjected to rigid body refinement against the combined X-ray and neutron scattering data using SASREF7.[19,24] This program uses the same simulated annealing method as SASREF6 to optimize the positions of component structures to scattering profiles while minimizing steric clashes, but has been generalized to handle neutron contrast variation data on protein complexes with deuterated components. All of the measured data to Q_{max}=0.3 Å^{-1} were used. Above this Q value the data are flat and noisy and do not contain any shape information on the protein components or the complex. The $KinA_2$ portion of the model was allowed flexibility between the CA domains and the DHp domain, whilst the Sda molecules were free to move with only a loose constraint to help orient them such that the surface implicated in binding[4] was directed towards $KinA_2$. The movement of the CA domain with respect to the DHp is likely to involve conformational changes in the linker sequence. The flexibility in the linker sequence was accomplished by allowing the CA domain to rotate freely about two different peptide bonds in the linker sequence (torsion between S319 and L320, and between R324 and E325 of the 2C2A coordinates). The use of two points of rotational freedom in the linker sequence allowed an expansive search for the optimal positions of the CA domains relative to the DHp to be performed, including allowing for sampling positions that stretched the CA domain to the

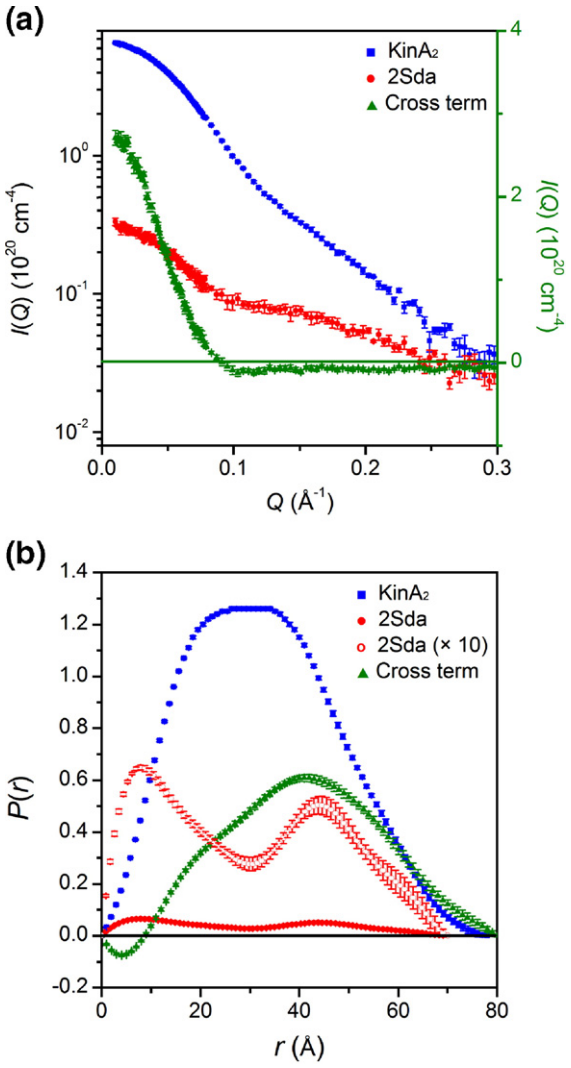

Figure 5. Component scattering functions corresponding to $KinA_2$, $2^{D}Sda$ and the cross term extracted from the neutron data (a), and corresponding $P(r)$ vector length distributions (b).

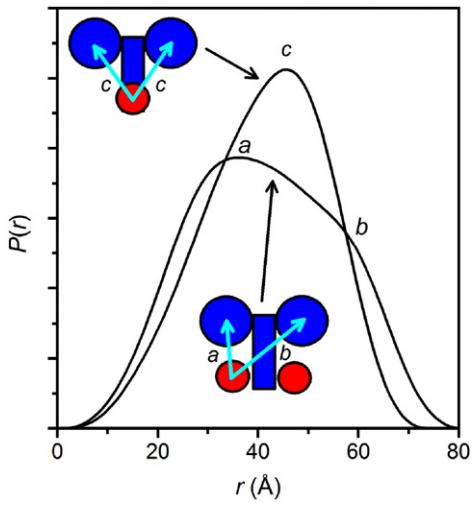

Figure 6. Two possible orientations of the Sda monomers with respect to the CA domain of the KinA. The vectors drawn onto the representations of the complex indicate how features of the $P(r)$ profile can be related to the structure.

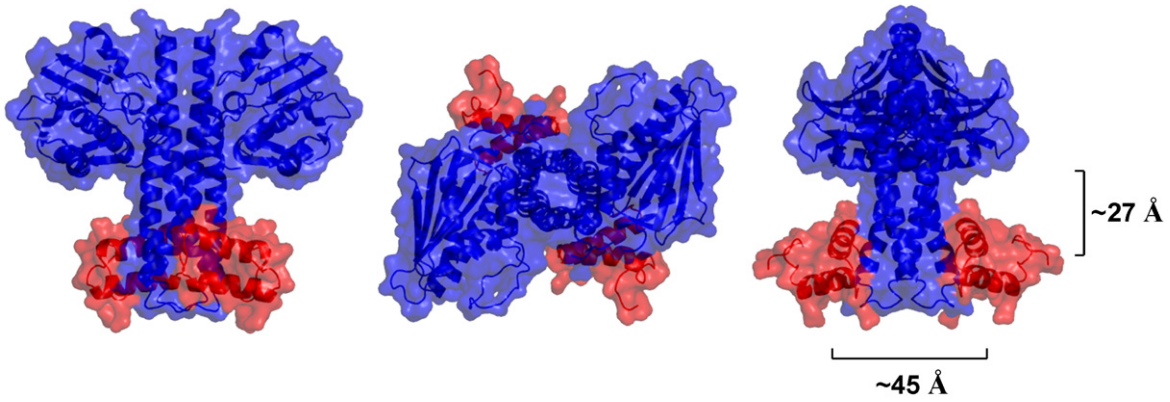

Figure 7. Best-fit model of the KinA dimer (blue surface and skeleton) complexed by two Sda molecules (red surface and skeleton) obtained from rigid-body modeling. Distances refer to the derived distances between the centers of mass of the two Sda molecules (~45 Å) and the distance between the centers of mass of the deuterated (Sda) and non-deuterated (KinA) components (~27 Å). Three perspectives are shown.

opposite end of the DHp stalk. The entire system was constrained by a 2-fold symmetry axis through the center of the four-helix bundle of the DHp domain. The simulated annealing calculation was repeated 14 times, and each of the minimized structures consistently positioned the CA domains and Sda molecules at opposing ends of the DHp stalk, with the Sda molecules slightly off-set from the plane perpendicular to the plane of the CA domains. The model that best fit to the scattering data (represented in Figure 7) gave χ^2 values equal to 0.97, 0.63, 0.56, 0.56, 0.92, 1.12, 0.95, 1.27 for the neutron data in 0, 10, 20, 40, 80, 90, 100% D_2O and the X-ray data, respectively. Two of the remaining minimized structures gave fits that were statistically as good as this best-fit model, and these had the same approximate dispositions for the KinA domains and Sda molecules. The remaining minimizations all gave models that had significantly worse steric clash penalties and fits, especially for the 100% D_2O data, which are dominated by the scattering from the $KinA_2$ component. Some of these remaining structures have the same relative positions of the CA domains and Sda molecules, but effectively rotated by ~90° with respect to the axis down the DHp stalk. Additional infrequent refinement outputs with relatively poor fits to the data were of models in which the CA domains and Sda molecules effectively swapped ends with respect to the length of the DHp stalk. These latter models had the Sda molecules positioned near the very end of the DHp stalk with a very restricted surface area of interaction between the Sda and DHp stalk that was not deemed meaningful. The sub-optimal characteristics of this interaction result from the fact that the DHp domain at the sensor end of the stalk is constructed of only two (not four) helices.

Ab initio shape restoration modeling of the complex was also performed using the combined X-ray and neutron scattering data and the program MONSA.[24,25] A typical dummy atom output from these calculations is displayed in Supplementary Data. None of the *ab initio* reconstructions fit the scattering data as well as the best-fit rigid body models. Nonetheless, the features identified are similar to those of our model presented in Figure 7. Specifically, the deuterated component (2^{D}Sda) is resolved in two positions towards the base of a T-shaped non-deuterated component ($KinA_2$); the deuterated species are rotated with respect to the bulky lobes corresponding to the CA domains; and, there is a significant separation between the centers of mass for the deuterated and non-deuterated components.

Our three best-fit models from our rigid-body refinements all show very similar arrangements of the domains and subunits, excellent χ^2 values with respect to all data sets, and have significantly lower steric clash penalties. In addition, they show excellent agreement with the structural parameters derived independently using the R_g analyses and scattering profile decomposition described above and are consistent with the general features of the *ab initio* shape restoration model.

The $KinA_2$-2Sda structure suggests an allosteric mechanism for inhibition

The scattering data support a model of the $KinA_2$-2Sda complex in which the CA domains of $KinA_2$ sit in a "non-active" conformation relative to the target histidine residues on the DHp stalk, and the Sda molecules are positioned at the base of this stalk (Figure 7). Although torsion within the hinge region has allowed placement of the CA domains such that they reflect the reduced D_{max} observed in the complex, the target histidine residues in our favored model are still accessible to the solvent and potentially the Spo0F protein (discussed below). The absence of steric overlap between the Sda molecules and the CA domains suggests that the inhibition of autokinase activity is not simply the result of Sda acting as a steric block, as might have been expected had the Sda proteins bound to the

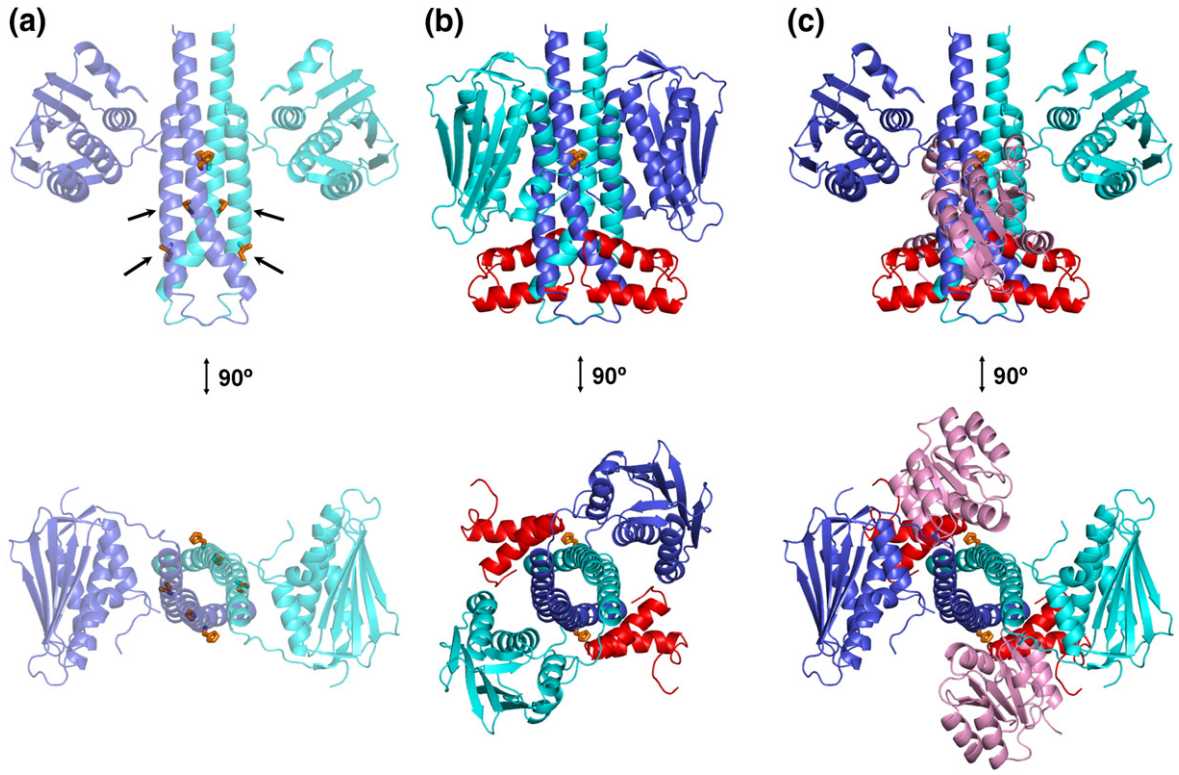

Figure 8. Models showing (a) the position of point mutants no longer capable of binding Sda (arrows and sticks); (b) the positioning of Sda molecules (red) in the context of catalytic domains poised for autokinase activity; (c) the positioning of Sda molecules in the context of Spo0F molecules (pink) poised for phosphotransfer. A stick representation of the target histidine is used in each case.

hinge region or to surfaces contributed by both the DHp and CA domains.

There is some genetic evidence that supports our scattering-derived model. A mutant of KinA was recently identified that has reduced affinity for Sda and retains wild-type autokinase activity (K. A. Cunningham and W. F. Burkholder, personal communication). The mutant has two missense mutations, P410L and F436S, corresponding to P265 and I296 in the HK853 structure. Residues P265 and I296 are located in the DHp domain of HK853 (on helices α1 and α2, respectively), further down the stalk from the target histidine (Figure 8(a), arrows). Whilst our model suggests it is unlikely that Sda interacts directly with these residues (compare Figure 8(a) and (b)), it is possible that conformational perturbations arising from the mutated residues could transmit positional adjustments down the stalk to the residues to which Sda specifically interacts.

Our $KinA_2$-2Sda model appears to place the Sda molecules out of reach of the CA domains. We did some additional modeling in order to assess the possibility that they can sterically restrict access of the CA domains to the target histidine residues by interfering with their movement into an active conformation. Using the targeted-crosslink model of the EnvZ CA domain catalytically poised on the DHp domain as a template,[12] it is possible to position the CA domains of $HK853_2$ in similar positions over the target histidine residues (H260) and associated DHp domain.[13] With the CA domains of $HK853_2$ modeled in this configuration (Figure 8(b)), there appears to be ample room for both the catalytically poised CA domains and Sda molecules (red ribbon) to occupy their positions on the DHp stalk simultaneously. Hence, it appears unlikely that Sda functions as a simple molecular barricade. An alternate possibility, particularly in light of the above-mentioned P410L and F436S point mutant findings, is that Sda exerts its effects *via* an allosteric mechanism, with the inhibitory signal transmitted through the DHp domain.

Finally, a criterion that a $KinA_2$-2Sda model should meet is the finding that Sda binding, whilst inhibiting autokinase activity, does not prevent phosphotransfer from KinA to Spo0F[4], the next protein in the phosphorelay. The structure of Spo0F has been solved in complex with Spo0B.[26] Although structurally similar to the HK853 dimer, the DHp domain of Spo0B is smaller and has a slightly different helix bundle arrangement (the helices within the bundle subtly screw to the right, not the left as in HK853). The helix that contributes the bulk of the contact surface with Spo0F, α1, is structurally very similar to the α1 helix of HK853. Superposing these helices allows for Spo0F molecules to be docked onto the HK853 dimer in positions suitable for the phosphotransfer event.[13] Figure 8(c) shows Spo0F (pink ribbon) modeled onto HK853 in just such a manner in the presence of Sda (red ribbon). In this case some steric overlap

between the Sda and Spo0F molecules is observed. If, as suggested by our preferred best-fit model, the Sda and Spo0F are mutually exclusive binders of KinA, then how could phosphotransfer to Spo0F be accomplished in the presence of Sda? Perhaps the competing equilibria at play (i.e. KinA-Sda and KinA-Spo0F association and dissociation, and CA movement between active and relaxed positions) are such that the CA domains are prevented from accessing the target histidine in the presence of either protein. Our rigid-body modeling calculations did yield some models for $KinA_2$-2Sda (described above) in which the CA and Sda components were rotated by 90° with respect to our preferred model. Although such arrangements place Sda molecules where they are no longer an impediment to Spo0F binding, Spo0F would still be prevented from accessing the target histidine due to the differently positioned CA domains. Hence, coupled with their fitting the scattering data less well, such alternate arrangements have been discounted.

Conclusion

Small-angle scattering has been used to analyze the histidine kinase KinA, its inhibitor, Sda, and the complex that they form. Both Sda alone and KinA alone have been found to be homodimers in solution. When they combine to form the $KinA_2$-2Sda complex, $KinA_2$ undergoes significant compaction compared to $KinA_2$ alone. When binding $KinA_2$, the Sda_2 dimer dissociates such that individual Sda molecules are available for binding. The Sda molecules have been shown to bind to the base of the DHp stalk of $KinA_2$ such that they do not interact with each other and are unlikely to interact directly with the CA domains.

The mechanism for the inhibition of KinA autokinase activity was originally proposed to involve Sda binding $KinA_2$ in such a manner as to prevent the CA domains of $KinA_2$ from accessing their target histidine residues.[4] This inhibition might have been achieved by an appropriately positioned Sda acting as a physical block to the movement of the CA domains, or by Sda binding and immobilizing the linking region connecting each CA domain to the DHp stalk. A recent prediction identifies hydrophobic residues towards the end of the α2 and α2′ helices of KinA protomers (adjacent to the hinge regions) as potential Sda binding sites.[15] The scattering experiments presented here best support a $KinA_2$-2Sda arrangement in which Sda is not in physical contact with either the CA domains of KinA, or with the hinge linking the CA domains to the DHp stalk. Hence, our model suggests that Sda may inhibit KinA autokinase activity *via* an allosteric signal transmitted *via* the four-helix bundle of the DHp domain, rather than by acting simply as a steric-block. The observation that Sda stabilizes KinA dimerization[4] is consistent with such a model, as are the identification of KinA point-mutations defective in Sda binding mapping in the vicinity of the Sda-binding site on the DHp stalk. Modulation of the autokinase activity of histidine kinases *via* conformational changes in the four-helix bundles of DHp domains has previously been suggested as a means by which signals from sensor domains of histidine kinases are transduced to CA domains. Signal transduction *via* DHp four-helix bundles might involve the concerted sliding ("helical piston displacement"[27]), tilting or twisting of helices.[28] Our model for $KinA_2$-2Sda suggests the intriguing possibility that such motions could play a role in transmitting an inhibitory signal.

Materials and Methods

Protein expression and purification

KinA protein was overexpressed from the pET28b-based plasmid pBB202[4] to yield a 245 amino acid residue protein containing the autocatalytic domain of KinA (residues 383–606) fused to a 21 residue N-terminal sequence comprising a 6His-tag and thrombin cleavage linker. Full-length protein had a predicted mass of 27,232 Da, with subsequent tag removal yielding a 228 residue protein of 25,350 Da. Sda was overexpressed from the pET28a-based plasmid pSLR65[4] to yield Sda (46 residues) fused *via* a thrombin linker to GST (from *Schistosoma japonicum*). Tag removal yielded Sda with two additional N-terminal residues (Gly-Ser) and a predicted mass of 5584 Da. Both proteins were overexpressed within an *E. coli* BL21(DE3) host induced during mid-exponential growth at 30 °C with 1 mM isopropyl-β-D-thiogalactopyranoside. Cultures expressing KinA and Sda were harvested 5 or 12 h post-induction, respectively.

Lysis of both strains was achieved in the presence of lysozyme (~100 μg/ml, United States Biochemical) by cycles of freeze-thaw and pressure shock in a buffer comprising 50 mM Tris(hydroxymethyl)aminomethane (Tris, pH 8.5), 50 mM NaCl and 1 mM phenylmethylsulphonyl fluoride. All subsequent steps were performed at room temperature. KinA was purified chromatographically by sequential passage over DEAE-agarose and Ni-NTA® resin (Qiagen, imidazole elution). Size-exclusion chromatography over a HiLoad® 16/60 Superdex 200 prep grade column attached to a BioLogic DuoFlow® FPLC (both BioRad) in Buffer A (50 mM Tris (pH 8.5), 50 mM NaCl, 150 mM imidazole) yielded protein ~98% pure, as judged by SDS-PAGE. Sda was purified by passage over DEAE-agarose followed by affinity chromatography on glutathione-agarose resin (glutathione elution). Off-column cleavage of the GST-tag with thrombin (Roche) was followed by size-exclusion chromatography as described for KinA, yielding Sda protein ~98% pure, as judged by SDS-PAGE.

The ^{D}Sda was produced by culturing cells in M9 salts minimal media dissolved in 97% (v/v) D_2O using non-deuterated glycerol as the carbon source. Cells were adapted to D_2O by using a single colony to inoculate a starter culture comprising 50% D_2O. Once an $A_{600\ nm}$ of 1.0 was achieved this culture was used to inoculate a 70% D_2O culture to an $A_{600\ nm}$ of 0.1. This procedure was repeated for 90% and 97% D_2O starter cultures, with the latter used to inoculate the preparative culture (4.5 l, 97% D_2O, to $A_{600\ nm}$ of 0.01). Induction of expression and purification of ^{D}Sda were performed as described above

for the non-deuterated Sda, however the reduced growth rates resulted in the harvest being performed 24 h post-induction. Post purification and GST-tag removal, this method yielded approximately 8 mg ^{D}Sda.

Whole-protein mass spectrometry

Protein solutions (50 μl) were desalted by dialysis against 50 mM Tris (pH 8.5). Samples (1 μl) were then spotted onto a target plate with an equal volume of α-cyano-4-hydroxycinnamic acid (10 mg/ml in 70% acetonitrile, 1% tri-fluoro-acetic acid) and air-dried at RT. Mass spectra were acquired in the mass:charge range of 1000–30,000 *m/z* on a QSTAR XL mass spectrometer equipped with a MALDI source (Applied Biosystems). Mass calibration was performed using Glu-fibrinopeptide B (Sigma) as an external calibrant.

Sample preparation for small-angle scattering experiments

Protein concentrations were estimated by spectrophotometry using calculated molar extinction coefficients at 280 nm (5120 $M^{-1}cm^{-1}$ for KinA and 1280 $M^{-1}cm^{-1}$ for Sda). The $KinA_2$-2Sda complex was formed by incubating a 1:2 molar ratio of KinA:Sda overnight at room temperature. Complex was separated from excess Sda by size-exclusion chromatography (described above) and the composition of fractions confirmed by SDS-PAGE.

Protein samples were concentrated using stirred cells (Millipore) or centrifuge concentrators (Pall) with 3 kDa molecular mass cut-offs. Samples used for X-ray scattering experiments were dialyzed against Buffer A, the filtrate of which was used for the solvent blank measurement. The post-dialysis protein concentrations of samples analyzed by X-ray scattering were: KinA, 3.7 mg/ml; Sda, 5.2 mg/ml; and KinA-Sda complex, 4.4 mg/ml. The monodispersity of all samples was confirmed by dynamic light scattering (Dynapro) prior to scattering experiments.

The $KinA_2$-2^{D}Sda samples used in the neutron scattering experiment were formed and purified as described above. Mass spectrometry of the ^{D}Sda component indicated that ~86% of non-exchangeable protons were substituted with deuterium. Mass spectrometry also revealed that the KinA components of both $KinA_2$-2Sda and $KinA_2$-2^{D}Sda complexes did not carry a 6His-tag. Two sets of samples were prepared for neutron contrast variation experiments. Both involved dialysis of 350–400 μl protein aliquots against buffers differing only in their concentrations of D_2O. For the first contrast series, 3.7 mg/ml protein samples were dialyzed against Buffer A with D_2O concentrations of 0, 10, 20, 70 (700 μl sample prepared for this sample), 80, 90, and 100% (v/v). The "high concentration" contrast series (0, 10, 20, 40, 80, 90, and 100% D_2O) used protein complex at 11.9 mg/ml for all samples except the 40% D_2O sample, which was 26.9 mg/ml. Additionally, the high concentration contrast series employed Buffer A containing 200 mM NaCl to counter potential inter-particle interference. All D_2O concentrations were confirmed by densitometry (DMA 5000 Density Meter, Anton-Paar).

Small-angle scattering

The scattering data presented in Figure 2 were collected at the Australian Nuclear Science and Technology Organisation (ANSTO, Lucas Heights, Australia) on a Bruker Nanostar instrument with a copper target ($\lambda = 1.5418$ Å), three-pinhole collimation and HiStar 2D detector with 100 μm resolution. 15 μl samples of protein or matched buffer solutions were sequentially mounted in the same sealed quartz capillary and irradiated for periods of 1 h per exposure at 20 °C. The sample to detector distance was 65 cm, giving a measurable Q-range of 0.02–0.34 $Å^{-1}$, where $Q = 4\pi(\sin\theta)/\lambda$, and θ is half the angle between the incident and scattered beams. Six 1 h exposures were acquired for the common buffer, while three, two, and five exposures were acquired for the $KinA_2$, Sda_2, and the $KinA_2$-2Sda complex, respectively. A lysozyme concentration series (6.5, 11.0, 17.5, and 22.0 mg/ml) was also measured so that analysis of $I(0)$ for each of the samples could yield information regarding the association state of the molecules in solution. Data for each exposure were corrected for non-uniform detector response and radially averaged to produce $I(Q)$ *versus* Q profiles using Bruker software. Multiple scattering profiles for each sample were averaged, and normalized buffer scattering data were subtracted to obtain the scattering profile for the protein using the program PRIMUS.[29] Additional X-ray scattering data characterising the deuterated protein samples and the weakly scattering, low concentration samples of Sda were collected at beamline 4-2 at the Stanford Synchrotron Radiation Laboratory (SSRL, Menlo Park, CA, USA). X-ray scattering data investigating inter-particle interference used the instruments at the University of Utah[30] (Utah, USA), and at the Australian National University (ACT, Australia).

Neutron scattering data were collected on the NG3 30 m SANS instrument at the National Institute for Standards and Technology (NIST, Gaithersburg, MD, USA)[31,32] using a neutron wavelength of 5.82(±0.04) Å and sample to detector distances of 1.33 m (detector offset by 25.00 cm, Q-range 0.03–0.45 $Å^{-1}$), and 5.00 m (detector centered, Q-range 0.01–0.09 $Å^{-1}$). For all experiments, data collection at 1.33 m was performed for half as long as collection at 5.0 m, with collection times at 5.0 m being: 3 h (0%), 3 h (10%), 1 h (20%), 1 h (70%), 1 h (80%), 1 h (90%) and 1 h (100%) for the low concentration samples; 2 h (0%), 2 h (10%), 2 h (20%), 2 h (40%), 1 h (80%), 1 h (90%) and 1 h (100%) for the high concentration samples. Samples and buffers were loaded in Hellma quartz cylindrical cells (outside diameter, 22 mm; path length, 1.00 mm, except for the 70% D_2O sample and buffer, which were loaded in 2.00 mm cells). All measurements were conducted at 20.0 °C. The two-dimensional data were normalised to a common incident neutron count (10^8 neutrons) and corrected for background counts, empty cell counts, and non-uniform detector response. The data were placed on an absolute scale by normalising the scattered intensity to the incident beam flux. The two-dimensional data were then radially averaged to produce $I(Q)$ *versus* Q profiles. The two data sets for each sample were then merged, with the high-Q data scaled relative to the low-Q data to remove any discontinuities between data sets. Normalized buffer scattering data were subtracted from the protein in buffer data to give the protein scattering profiles. Due to the effects of incoherent scattering by the H-rich samples and small variations between quartz cells, the background levels in the high-Q portion of the various buffer-corrected scattering profiles showed small differences. To correct for these effects a constant was subtracted from all samples such that the average background level for $0.35 < Q < 0.40$ $Å^{-1}$ for all samples was the same as the 80% data, which conformed well to

the expected Q^{-4} dependence of the scattering profile at high-Q for proteins in solution.[33] The R_g and $I(0)$ values were estimated by Guinier analysis, using PRIMUS[29] and by indirect Fourier transformation of the data, using the program GNOM.[16] Decomposition of the scattering profiles and analysis of the contrast dependence of R_g values (using Sturhmann analysis and parallel axis theorem) were done using the methods previously described[21] and were performed using specific purpose-written software, using standard weighted least-squares fitting procedures.

Sequence alignment software

Amino acid alignments between KinA and homologues was performed with BLASTP (v2.2.14)[34] and MAFFT (v5.743).[35] Structural homology was analyzed with the Dali server.[36]

Acknowledgements

This research was supported in part by NHMRC Project Grant ID352434 awarded to G.F.K. and J.M. G. Additional support was provided in part by the Office of Science (BER), U. S. Department of Energy, Grant No. DE-FG02-05ER64026 and ARC Federation Fellowship to J.T. We acknowledge the support of the National Institute of Standards and Technology, U.S. Department of Commerce, in providing the neutron research facilities used in this work. This work utilized facilities supported in part by the National Science Foundation under Agreement No. DMR-0454672. Portions of this research were carried out at the Stanford Synchrotron Radiation Laboratory, a national user facility operated by Stanford University on behalf of the U.S. Department of Energy, Office of Basic Energy Sciences. The SSRL Structural Molecular Biology Program is supported by the Department of Energy, Office of Biological and Environmental Research, and by the National Institutes of Health, National Center for Research Resources, Biomedical Technology Program. Travel was supported by the ANSTO Access to Major Research Facilities Programme (grant numbers 06/07-N-13 and 05/06-N-28), and access to X-ray facilities at ANSTO was supported by AINSE project number AINGRA06257. We thank Katherine A. Cunningham and William F. Burkholder for kindly communicating results prior to publication, and Susan L. Rowland for providing strains and plasmids. We thank Ben Crossett for performing Mass spectrometry using the Australian Proteome Analysis Facility established under the Australian Government's Major National Facilities program. We thank Michael Benovic (ANSTO) for helpfulness with heavy water. We thank John White and Duncan McGillivray (Australian National University) for assistance in obtaining X-ray scattering data needed to confirm that our higher protein concentration samples were free of inter-particle interference effects.

Supplementary Data

Supplementary data associated with this article can be found, in the online version, at doi:10.1016/j.jmb.2007.01.064

References

1. Hoch, J. A. (2000). Two-component and phosphorelay signal transduction. *Curr. Opin. Microbiol.* **3**, 165–170.
2. Piggot, P. J. & Hilbert, D. W. (2004). Sporulation of *Bacillus subtilis*. *Curr. Opin. Microbiol.* **7**, 579–586.
3. Burkholder, W. F., Kurtser, I. & Grossman, A. D. (2001). Replication initiation proteins regulate a developmental checkpoint in *Bacillus subtilis*. *Cell*, **104**, 269–279.
4. Rowland, S. L., Burkholder, W. F., Cunningham, K. A., Maciejewski, M. W., Grossman, A. D. & King, G. F. (2004). Structure and mechanism of action of Sda, an inhibitor of the histidine kinases that regulate initiation of sporulation in *Bacillus subtilis*. *Mol. Cell*, **13**, 689–701.
5. Taylor, B. L. & Zhulin, I. B. (1999). PAS domains: internal sensors of oxygen, redox potential, and light. *Microbiol. Mol. Biol. Rev.* **63**, 479–506.
6. Tanaka, T., Saha, S. K., Tomomori, C., Ishima, R., Liu, D., Tong, K. I. *et al.* (1998). NMR structure of the histidine kinase domain of the *E. coli* osmosensor EnvZ. *Nature*, **396**, 88–92.
7. Song, Y., Peisach, D., Pioszak, A. A., Xu, Z. & Ninfa, A. J. (2004). Crystal structure of the C-terminal domain of the two-component system transmitter protein nitrogen regulator II (NRII; NtrB), regulator of nitrogen assimilation in *Escherichia coli*. *Biochemistry*, **43**, 6670–6678.
8. Marina, A., Mott, C., Auyzenberg, A., Hendrickson, W. A. & Waldburger, C. D. (2001). Structural and mutational analysis of the PhoQ histidine kinase catalytic domain. Insight into the reaction mechanism. *J. Biol. Chem.* **276**, 41182–41190.
9. Bilwes, A. M., Alex, L. A., Crane, B. R. & Simon, M. I. (1999). Structure of CheA, a signal-transducing histidine kinase. *Cell*, **96**, 131–141.
10. Nowak, E., Panjikar, S., Morth, J. P., Jordanova, R., Svergun, D. I. & Tucker, P. A. (2006). Structural and functional aspects of the sensor histidine kinase PrrB from *Mycobacterium tuberculosis*. *Structure*, **14**, 275–285.
11. Tomomori, C., Tanaka, T., Dutta, R., Park, H., Saha, S. K., Zhu, Y. *et al.* (1999). Solution structure of the homodimeric core domain of *Escherichia coli* histidine kinase EnvZ. *Nature Struct. Biol.* **6**, 729–734.
12. Cai, S. J., Khorchid, A., Ikura, M. & Inouye, M. (2003). Probing catalytically essential domain orientation in histidine kinase EnvZ by targeted disulfide cross-linking. *J. Mol. Biol.* **328**, 409–418.
13. Marina, A., Waldburger, C. D. & Hendrickson, W. A. (2005). Structure of the entire cytoplasmic portion of a sensor histidine-kinase protein. *EMBO J.* **24**, 4247–4259.
14. Yamada, S., Akiyama, S., Sugimoto, H., Kumita, H., Ito, K., Fujisawa, T. *et al.* (2006). The signaling pathway in histidine kinase and the response regulator complex revealed by X-ray crystallography and solution scattering. *J. Mol. Biol.* **362**, 123–139.
15. Varughese, K. I., Tsigelny, I. & Zhao, H. (2006). The crystal structure of beryllofluoride Spo0F in complex with the phosphotransferase Spo0B represents a phosphotransfer pretransition state. *J. Bacteriol.* **188**, 4970–4977.

16. Svergun, D. (1992). Determination of the regularization parameter in indirect-transform methods using perceptual criteria. *J. Appl. Crystallog.* **25,** 495–503.
17. Guinier. (1939). La diffraction des rayons X aux tres petits angles; application a l'etude de phenomenes ultramicroscopiques. *Ann. Phys.* **12**, 161–237.
18. Svergun, D. I., Barberato, C. & Koch, M. H. (1995). CRYSOL - a program to evaluate X-ray solution scattering of biological macromolecules from atomic coordinates. *J. Appl. Crystallog.* **28**, 768–773.
19. Petoukhov, M. V. & Svergun, D. I. (2005). Global rigid body modeling of macromolecular complexes against small-angle scattering data. *Biophys. J.* **89**, 1237–1250.
20. Ibel, K. & Stuhrmann, H. B. (1975). Comparison of neutron and X-ray scattering of dilute myoglobin solutions. *J. Mol. Biol.* **93**, 255–265.
21. Olah, G. A., Rokop, S. E., Wang, C. L., Blechner, S. L. & Trewhella, J. (1994). Troponin I encompasses an extended troponin C in the Ca(2+)-bound complex: a small-angle X-ray and neutron scattering study. *Biochemistry*, **33**, 8233–8239.
22. Moore, P. B., Engelman, D. M. & Schoenborn, B. P. (1974). Asymmetry in the 50S ribosomal subunit of *Escherichia coli*. *Proc. Natl Acad. Sci. USA*, **71**, 172–176.
23. Tsai, J., Taylor, R., Chothia, C. & Gerstein, M. (1999). The packing density in proteins: standard radii and volumes. *J. Mol. Biol.* **290**, 253–266.
24. Petoukhov, M. V. & Svergun, D. I. (2006). Joint use of small-angle X-ray and neutron scattering to study biological macromolecules in solution. *Eur. Biophys. J.* **35**, 567–576.
25. Svergun, D. I. (1999). Restoring low resolution structure of biological macromolecules from solution scattering using simulated annealing. *Biophys. J.* **76**, 2879–2886.
26. Zapf, J., Sen, U., Madhusudan, Hoch, J. A. & Varughese, K. I. (2000). A transient interaction between two phosphorelay proteins trapped in a crystal lattice reveals the mechanism of molecular recognition and phosphotransfer in signal transduction. *Structure*, **8**, 851–862.
27. Falke, J. J. & Hazelbauer, G. L. (2001). Transmembrane signaling in bacterial chemoreceptors. *Trends Biochem. Sci.* **26**, 257–265.
28. Cochran, A. G. & Kim, P. S. (1996). Imitation of *Escherichia coli* aspartate receptor signaling in engineered dimers of the cytoplasmic domain. *Science*, **271**, 1113–1116.
29. Konarev, P., Volkov, V. V., Sokolova, A. V., Koch, M. H. J. & Svergun, D. I. (2003). Primus: a Windows Pc-based system for small-angle scattering data analysis. *J. Appl. Crystallog.* **36**, 1277–1282.
30. Heidorn, D. B. & Trewhella, J. (1988). Comparison of the crystal and solution structures of calmodulin and troponin C. *Biochemistry*, **27**, 909–915.
31. Glinka, C. J., Barker, J. G., Hammouda, B., Krueger, S., Moyer, J. J. & Orts, W. J. (1998). The 30 m small-angle neutron scattering instruments at the National Institute of Standards and Technology. *J. Appl. Crystallog.* **31**, 430–445.
32. Kline, S. R. (2006). Reduction and analysis of SANS and USANS data using Igor Pro. *J. Appl. Crystallog.* **39**, 895–900.
33. Porod, G. (1951). Die Röntgenkleinwinkelstreuung von dichtgepackten kolloiden systemen. *Kolloid-Zeitschrift und Zeitschrift fur Polymere*, **124**, 83–114.
34. Altschul, S. F., Madden, T. L., Schaffer, A. A., Zhang, J., Zhang, Z., Miller, W. & Lipman, D. J. (1997). Gapped BLAST and PSI-BLAST: a new generation of protein database search programs. *Nucl. Acids Res.* **25**, 3389–3402.
35. Katoh, K., Kuma, K., Toh, H. & Miyata, T. (2005). MAFFT version 5: improvement in accuracy of multiple sequence alignment. *Nucl. Acids Res.* **33**, 511–518.
36. Holm, L. & Sander, C. (1995). Dali: a network tool for protein structure comparison. *Trends Biochem. Sci.* **20**, 478–480.

Edited by K. Morikawa

(Received 21 December 2006; received in revised form 25 January 2007; accepted 26 January 2007)
Available online 3 February 2007